

Article

Facile Synthesis and Electrochemical Characterization of Polyaniline@TiO₂-CuO Ternary Composite as Electrodes for Supercapacitor Applications

Nadia Boutaleb ¹, Fatima Zohra Dahou ², Halima Djelad ³, Lilia Sabantina ^{4,*} , Imane Moulefera ⁵  and Abdelghani Benyoucef ^{6,*} 

¹ Department of Chemistry, Faculty of Science, University of Dr. Moulay Tahar, Saida 20000, Algeria

² Physics Department, Faculty of Exact Sciences, University of Mustapha Stambouli, Mascara 29000, Algeria

³ Department of Physical Chemistry, Institute of Materials, University of Alicante, 03080 Alicante, Spain

⁴ Junior Research Group “Nanomaterials”, Faculty of Engineering and Mathematics, Bielefeld University of Applied Sciences, 33619 Bielefeld, Germany

⁵ Chemical Engineering Department, Campus Universitario de Espinardo, University of Murcia, 30100 Murcia, Spain

⁶ L.S.T.E. Laboratory, Faculty of science and technology, University of Mustapha Stambouli, Mascara 29000, Algeria

* Correspondence: lilia.sabantina@fh-bielefeld.de (L.S.); a.benyoucef@univ-mascara.dz (A.B.)

Abstract: This research reports the facile, controlled, low-cost fabrication, and evaluation of properties of polyaniline matrix deposited on titanium dioxide and copper(II) oxide ternary-composite (PANI@TiO₂-CuO)-based electrode material for supercapacitor application. The process involves the preparation of CuO in the presence of TiO₂ to form TiO₂-CuO by a facile method, followed by in-situ oxidative polymerization of aniline monomer. The structural and physical properties were evaluated based on the results of FTIR spectroscopy, X-ray diffraction (XRD) analysis, X-ray photoelectron spectroscopy (XPS), transmission electron (TEM) and scanning electron (SEM) microscopy, thermogravimetric analysis (TGA), and BET surface areas analysis. The results indicated that TiO₂-CuO was dispersed uniformly in the PANI matrix. Owing to such dispersion of TiO₂-CuO, the PANI@TiO₂-CuO material exhibits dramatic improvements on thermal stability in comparison with the pure PANI. The cyclic voltammetry (CV) confirms the reversibility of PANI redox transitions for this optimized electrode material. Moreover, the results reveal that the specific capacitance of PANI@TiO₂-CuO reaches 87.5% retention after 1500 cycles under 1.0 A g⁻¹, with a better charge storage performance as compared to pure PANI and PANI@TiO₂ electrodes. The preparation of PANI@TiO₂-CuO with enhanced electrochemical properties provides a feasible route for promoting its applications in supercapacitors.

Keywords: copper(II) oxide; titanium dioxide; polyaniline; ternary-composite; supercapacitors



Citation: Boutaleb, N.; Dahou, F.Z.; Djelad, H.; Sabantina, L.; Moulefera, I.; Benyoucef, A. Facile Synthesis and Electrochemical Characterization of Polyaniline@TiO₂-CuO Ternary Composite as Electrodes for Supercapacitor Applications. *Polymers* **2022**, *14*, 4562. <https://doi.org/10.3390/polym14214562>

Academic Editor: Hai-Feng (Frank) Ji

Received: 6 October 2022

Accepted: 21 October 2022

Published: 27 October 2022

Publisher's Note: MDPI stays neutral with regard to jurisdictional claims in published maps and institutional affiliations.



Copyright: © 2022 by the authors. Licensee MDPI, Basel, Switzerland. This article is an open access article distributed under the terms and conditions of the Creative Commons Attribution (CC BY) license (<https://creativecommons.org/licenses/by/4.0/>).

1. Introduction

Recently, hybrid material composites have been extensively studied, owing to their potential utilities. They contain the unique properties of nanofillers, driving the materials with improved properties [1–3]. Moreover, conductive polymers (CPs) and their composites receive considerable attention due to their magnetic, optical, and opto-electronic characteristics [4,5]. Polyaniline (PANI) is one of the most common conducting polymers due to its distinct environmental stability, superior chemical/physical properties, thermal stability, ease to synthesis, and reversible doping/dedoping process [6–8]. They are commercially important polymers used extensively in many applications [9,10]. In recent years, hybrid materials based on CPs and inorganic materials have been investigated at length by incorporating the inorganic materials in a CP matrix. Furthermore, the final properties of nanocomposites depend not only on the properties of the individual components, but

also on the homogeneity of the dispersibility of the inorganics, and the interfacial between the interacted components [11,12]. On the other hand, to improve environmental stability, the metal oxide (MO) nanoparticles were added into CPs. The development of established technology is a result of the hybridization of nanocomposite to build an outstanding nanomaterial with specific features that outweigh the sum of their individual contributions [13]; because of their higher degradation efficiency, good physical and chemical properties, and low toxicity, CPs@MO nanomaterials have fascinated researchers for their excellent properties [13–15]. Among MOs, Titania (TiO_2) is a promising product because it is abundantly available in nature and is environmentally friendly [15–17]. As a suitable potential candidate, it has already been authorized in a broad range of different applications such as sensors, photocatalysis, solar cell, and anticorrosion [18]. Researchers have proclaimed the structural, optical, and electrical properties of PANI-based TiO_2 nanomaterials as an electrode material for supercapacitors, such as Deshmukh et al. [19] proved that the distinctive structure of the PANI- TiO_2 composite and the cohabitation of conducting PANI with TiO_2 have been found to be responsible for the superior electrochemical properties. Ghahramani et al. [20] synthesized PANI-coated reduced graphene oxide for removal of malachite green from aqueous solution. According to the results of Yoruk et al. [21], the rGO/ TiO_2 /PANI nanocomposite shows much better performance than its individual components in terms of specific capacitance, energy density, power density, and cycle life. Nevertheless, copper oxide (CuO) is also a p-type semi-conductor and has a narrow band gap of 1.2–1.9 eV, as well as high surface areas and unusual morphology structures, which provides it with characteristic physical and chemical properties that have been utilized in a number of applications such as magnetic storage, energy storage, photocatalysis, energy conversions, superconductors, solar cells, antimicrobial agents, and gas sensors [22,23]. Moreover, PANI, TiO_2 , and CuO can supplement each other and their synergistic effect can improve the performance of the hybrid material of PANI@ TiO_2 -CuO. For instance, Nekooie et al. fabricated a CuO/ TiO_2 /PANI to obtain a composite for chlorpyrifos depollution in water by visible light irradiation [24]. Pang et al.'s TiO_2 -SiO₂ and CuO- TiO_2 -SiO₂ nanocomposite fibers were formed by electrospinning with subsequent calcination. Then, in-situ chemical oxidative polymerization of aniline monomer was carried out with inorganic (TiO_2 -SiO₂ and CuO- TiO_2 -SiO₂) nanocomposite fibers as templates [25].

Presently, the ternary nanocomposite is becoming an emerging area of research. In our present work, we have prepared PANI@ TiO_2 -CuO via an in-situ chemical oxidative polymerization method. Relatively cheap and less hazardous raw materials are used for the synthesis, and thus make this process both economic and eco-friendly. The interaction phenomenon between PANI and CuO with TiO_2 was proven by XPS, FTIR, XRD, UV-vis, BET, TGA, TEM, and SEM techniques. Moreover, cyclic voltammetry (CV) was applied to study the electrochemical behavior of samples. Meanwhile, TiO_2 was used as an active material to prepare electrodes for use as a high-performance supercapacitor.

2. Materials and Method

2.1. Materials

Deionized water was used to produce all products. The copper nitrate ($\text{Cu}(\text{NO}_3)_2 \cdot 3\text{H}_2\text{O}$), ammonium persulfate, aniline, titanium (IV) oxide (TiO_2) ($\geq 99.98\%$), poly(vinylidene fluoride) (CH_2CF_2)_n ammonia solution (NH_4OH), N-methyl-2-pyrrolidone ($\text{C}_5\text{H}_9\text{NO}$), and hydrochloric acid (HCl) were procured from Sigma-Aldrich Chemical (Madrid, Spain). The sodium hydroxide (NaOH) and ethanol ($\text{C}_2\text{H}_5\text{OH}$) were purchased from Merck (Milan, Italy).

2.2. Fabricating TiO_2 -CuO Binary Composite

The TiO_2 -CuO composite was prepared as reported by Nguyen et al. [26]. 1 mmol of TiO_2 was dispersed in 25 mL of absolute $\text{C}_2\text{H}_5\text{OH}$ at 25 °C. Then, 25 mL of $\text{Cu}(\text{NO}_3)_2$ (0.02 M) were added to the solution suspension and stirred continuously for approximately 2 h at 500 rpm. Next, 0.25 M NaOH was added dropwise to this solution in order to adjust

the pH to 10. After stirring for another hour, the resulting black TiO₂–CuO precipitate was washed with deionized water and C₂H₅OH and the composite was dried at 70 °C in air for 5 h, and calcined at 400 °C for 3 h in air.

2.3. Synthesis of PANI@TiO₂-CuO Ternary Composite

Two solutions were prepared. Solution-(A): 1.16 g of TiO₂–CuO and 4.65 g of aniline were added into the 250 mL flask containing (1 M) HCl and stirred under ultrasonic for at least 1 h. Solution-(B): An amount of 11.50 g of ammonium persulfate was dissolved in 200 mL of 1 M HCl. Solution-(B) was then added to the aforementioned solution-(A), drop by drop, under constant magnetic stirring for another 24 h at a low temperature, allowing the aniline monomer polymerization and the obtainment of PANI@TiO₂–CuO sample. The PANI was prepared under the same conditions but without TiO₂–CuO, and also PANI@TiO₂ with the presence of the TiO₂ only [11,13,27].

2.4. Measurements

The chemical structure was characterized by FTIR (Bruker Instruments, Karlsruhe, Germany). The surface morphology of samples was characterized using SEM (JEOL JSM-5400, JEOL Ltd., Tokyo, Japan). The morphology of samples was further investigated by transmission electron microscopy (TEM) (JEOL-JEM 2100, JEOL Ltd., Tokyo, Japan). The surface composition was examined by X-ray photoelectron spectroscopy (XPS) analyses, utilizing a monochromatic 150 W Al X-ray source (ThermoScientific, Kyoto, Japan). The products were subjected to thermogravimetric analysis (TGA) technique (Hitachi-STA7200, Tokyo, Japan) under an N₂ atmosphere. The products were heated from 25 °C to 900 °C at a heating rate of 10 °C/min. The optical properties and concentration of materials in the solutions was determined by Hitachi-U3000 spectrophotometer (Hitachi High Technologies Corporation, Tokyo, Japan). The crystalline property was evaluated using a Bruker CCD-Apex diffractometer (Bruker Corporation, Madison, WI, USA) (scanning voltage: 40 kV, scanning current: 30 mA, scanning angle: 5~70°, scanning speed: 5° min⁻¹). The surface areas (S_{BET}) of the samples were determined by N₂ sorption–desorption on a Micrometrics ASAP 2420 analyzer (Micrometrics, Norcross, GA, USA) at 77 K using the Brunauer-Emmett-Teller method. Micropore volume and micropore surface area were estimated by the t-plot technique. The total pore volume (V_{total}) of pores was determined from the N₂ isotherms at $\frac{p}{p^0} = 0.99$.

2.5. Electrochemical Investigation

The electrochemical properties of the product electrodes were tested by cyclic voltammetry (CV) using a conventional three electrodes electrochemical system using an eDAQ Model EA163 potentiostat [27]. Moreover, the electrochemical measurements were carried out by performing galvanostatic charge/discharge (GCD) analyses. The working electrodes were produced via coating of stainless steel (SS) current collectors with homogenous slurry of PANI@TiO₂–CuO (80%) with carbon black (15 wt%) and CH₂CF₂_n (5 wt%) in C₅H₉NO. The synthesized electrodes were dried in a vacuum oven at 70 °C for one night.

3. Results

3.1. Structure and Morphology Analysis

The XRD patterns of samples are investigated (Figure 1a). The XRD pattern of PANI exhibits the XRD peaks at $2\theta = 20.2^\circ$, 25.03° and 28.69° [13]. These diffraction patterns proved the presence of crystalline domains in the amorphous PANI structure. The XRD patterns of crystalline CuO have characteristic diffraction peaks at 2θ values of 32.76° , 35.66° , 38.93° , 48.79° , 53.67° , 58.26° , 61.62° , 66.59° , and 68.22° , corresponding to (110), (002), (111), (202), (020), (202), (113), (311), and (220) lattice planes, respectively (JCPDS: 48-1548). Moreover, the characteristic peaks of TiO₂ appear at 25.3° , 36.88° , 37.78° , 38.61° , 48.04° , 53.92° , 55.05° , 62.70° , and 68.85° , which can be attributed to the (101), (103), (004), (112), (200), (105), (211), (204), and (110) crystal planes, respectively [17,27]. Furthermore,

the peaks diffraction pattern of the $\text{TiO}_2\text{-CuO}$ are a combination of signals from both TiO_2 (JCPDS: 89-4921) and CuO (JCPDS: 48-1548), showing the crystal morphology and successful preparation of the $\text{TiO}_2\text{-CuO}$ structure. The XRD patterns of $\text{PANI@TiO}_2\text{-CuO}$ have the feature peaks of the PANI, as well as some peaks associated with $\text{TiO}_2\text{-CuO}$. This proves the introduction of crystallinity to the PANI matrix and validates the preparation of hybrid material. From the characteristic diffraction, it appears that the broadness of XRD peaks of PANI is reduced and moved to higher 2θ values with respect to pure PANI. For instance, the peaks at 20.21° and 24.85° are slightly shifted to 20.62° and 24.97° for $\text{PANI@TiO}_2\text{-CuO}$, respectively. This is attributed to the stronger coordination binding between the $\text{TiO}_2\text{-CuO}$ composite and the PANI matrix.

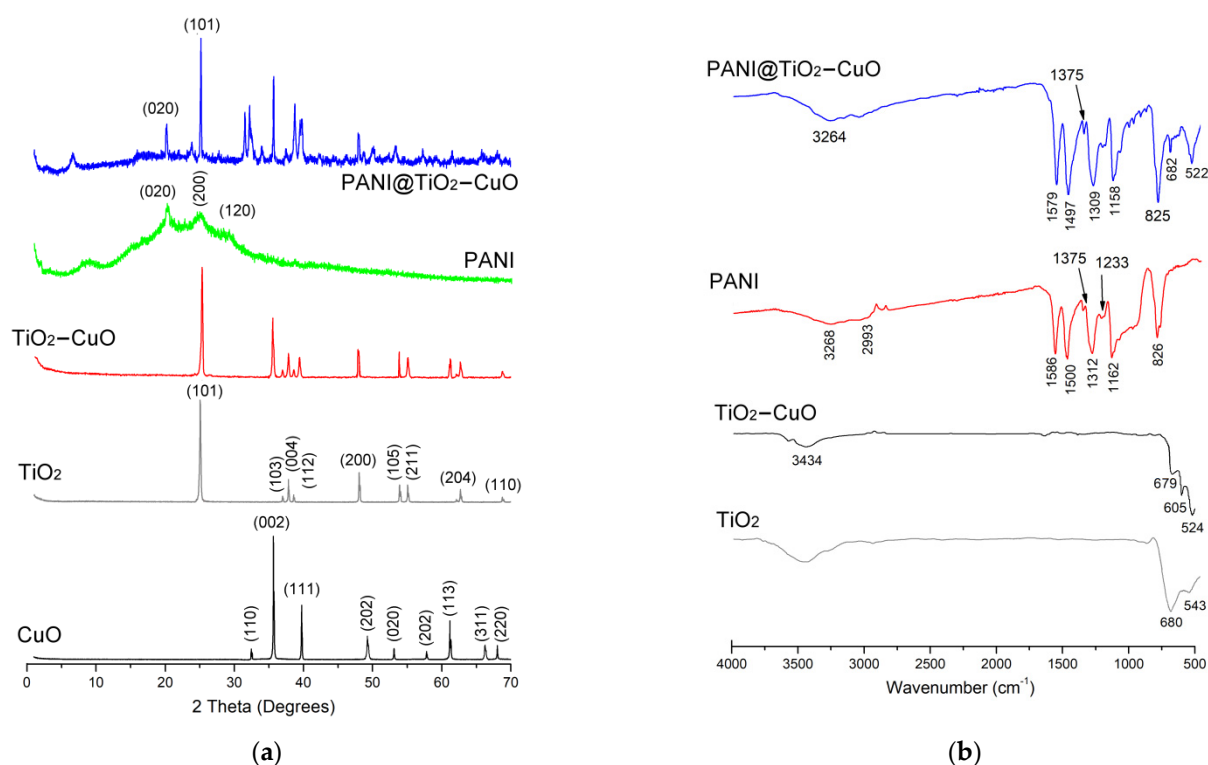


Figure 1. (a): XRD patterns and (b): FTIR analysis of samples.

The FTIR spectra of samples are shown in Figure 1b. As seen in the FTIR spectra, the TiO_2 presented signals around 3439 cm^{-1} assigned to angular deformation of adsorbed water and TiO_2 structure with a strong band between 543 cm^{-1} and 680 cm^{-1} [27]. In addition, the FTIR spectra of $\text{TiO}_2\text{-CuO}$ exhibit three vibrations occurring at 524 cm^{-1} , 605 cm^{-1} , and 679 cm^{-1} for this sample, which can be attributed to the vibrations of Cu-O with TiO_2 , confirming the formation of highly $\text{TiO}_2\text{-CuO}$ composite. Moreover, PANI shows typical peaks at 1586 cm^{-1} , 1500 cm^{-1} , 1375 cm^{-1} , 1312 cm^{-1} , 1162 cm^{-1} and 826 cm^{-1} related to the stretching of the nitrogen quinone (Q) structure, benzene ring (B) structure vibration, C-N⁺ vibration, C-N vibration, in-plane C-H vibration, and out-of-plane C-H bending vibrations, respectively [28]. Compared with the FTIR spectra of hybrid material, the main change in the FTIR spectra of $\text{PANI@TiO}_2\text{-CuO}$ is the apparition of all bands of PANI with two new bands at 682 cm^{-1} and 522 cm^{-1} , that confirms the incorporation of polymer matrix in $\text{TiO}_2\text{-CuO}$ composite.

According to the XPS analysis (Figure 2a), the elements had been changed during the synthesis process, and compared with PANI, the XPS spectrum of $\text{PANI@TiO}_2\text{-CuO}$ new peaks Ti2p, Ti2s, Cu2p, and Cu3p related to $\text{TiO}_2\text{-CuO}$ composite. Moreover, the O/C ratio of PANI was lower than that of $\text{PANI@TiO}_2\text{-CuO}$, proving the presence of bi-metal oxide in the PANI matrix.

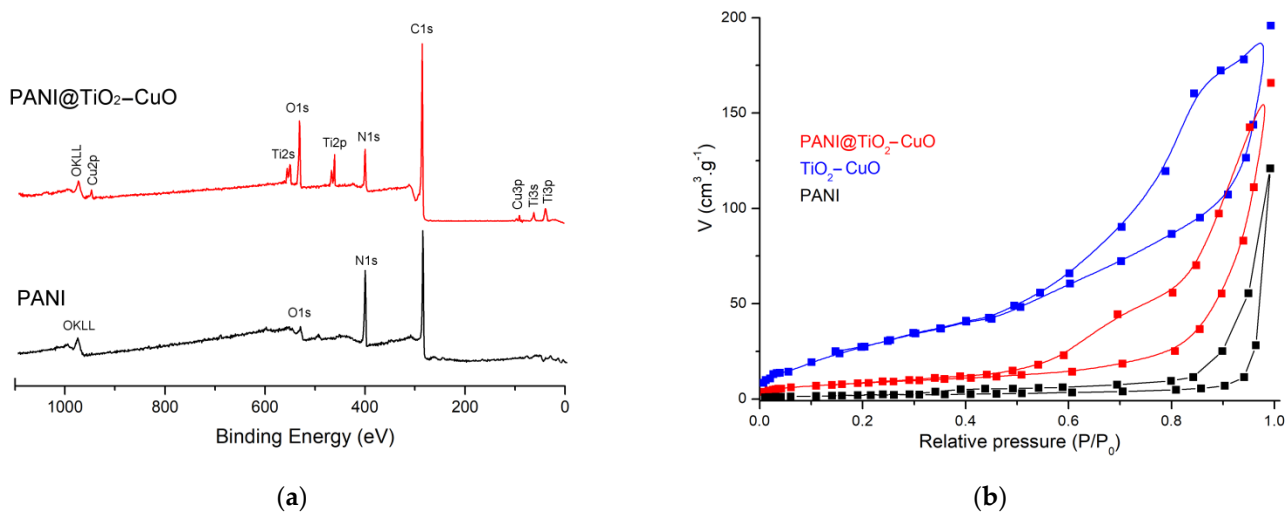


Figure 2. (a): Survey XPS spectra and (b): N₂ sorption isotherms of samples.

Furthermore, as can be seen in Figure 3a, the high spectral resolution of the C1s peak for PANI showed three sub-peaks at 284.26 eV, 285.66 eV and 286.09 eV, which were assigned to the C–C/C–H, C–N and C=N bonds, respectively. The high-resolution spectra of ternary composite for N1s (Figure 3b) displayed two sub-peaks at 398.97 eV and 400.28 eV related to –N= and –NH–, respectively [29,30]. However, after the loading of polymer matrix onto the surface of TiO₂–CuO, the C1s peak of PANI@TiO₂–CuO showed a negative/positive shift in the binding energy compared to PANI; this spectrum (Figure 3c) reveals the existence of four peaks, namely 284.68 eV (C–C and C–H), 285.60 eV (C–N), 286.14 eV (C=N) and 287.19 eV (C=O). Further, the three peaks delimited in the N1s spectrum of PANI (Figure 3d) are considered as –N= (398.39 eV), –NH– (399.53 eV) and the –NH⁺ = peak at 400.35 eV, respectively [27,31]. Thus, these results demonstrate that polymers were successfully formed on the TiO₂–CuO surface.

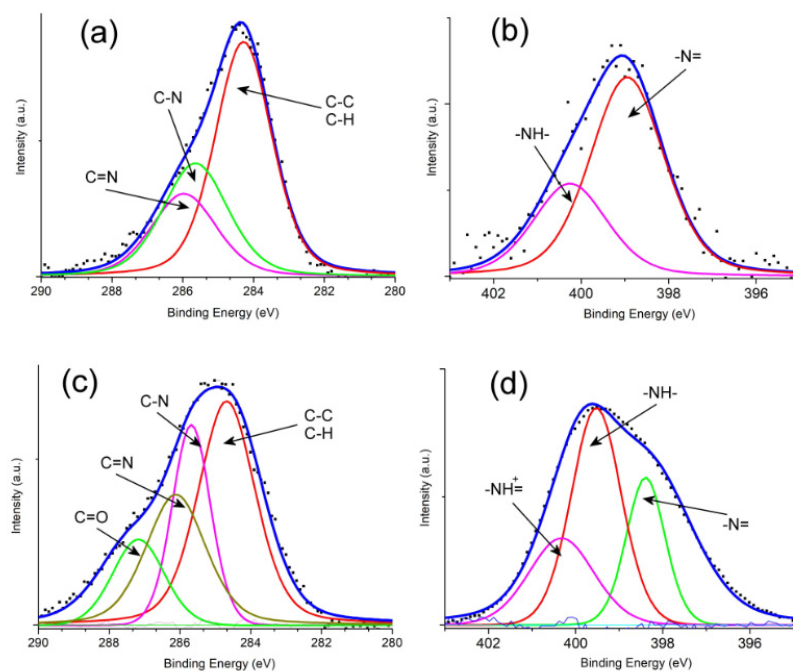


Figure 3. XPS spectral signals: (a) C1s of PANI, (b) C1s of PANI@TiO₂–CuO, (c) N1s of PANI@TiO₂–CuO, and (d) N1s of PANI.

The N₂ adsorption–desorption isotherms for PANI, TiO₂–CuO and PANI@TiO₂–CuO are presented in Figure 2b. It can be observed that all of the samples presented isotherms that are typical of mesoporous materials [32]. BET surface area (S_{BET}) and total pore volume (V_{total}) for samples are listed in Table 1. From the data, it can be inferred that S_{BET} and V_{total} of TiO₂–CuO decreased after the PANI matrix formation on the TiO₂–CuO surface, indicating that the polymer was created on the TiO₂–CuO pore structure; similar behavior was also observed by Toumi et al. [33]. Moreover, PANI@TiO₂–CuO presented a higher surface area than pure PANI.

Table 1. Materials’ textural characteristics obtained from N₂ adsorption-desorption data.

Material	PANI	PANI@TiO ₂	TiO ₂ –CuO	PANI@TiO ₂ –CuO
$S_{\text{BET}}/(\text{m}^2 \text{g}^{-1})$	25 ± 0.5	53 ± 0.5	132 ± 0.5	108 ± 0.5
$V_{\text{DR}}(\text{N}_2)/(\text{cm}^3 \text{g}^{-1})$	1.50 ± 0.01	1.32 ± 0.01	1.98 ± 0.01	1.94 ± 0.01
$V_{\text{meso}}/(\text{cm}^3 \text{g}^{-1})$	0.01	0.02	0.05	0.04
$V_{\text{macro}}/(\text{cm}^3 \text{g}^{-1})$	0.01	0.08	0.14	0.11
$V_{\text{tot pore}}/(\text{cm}^3 \text{g}^{-1})$	0.02	0.10	0.19	0.15

SEM was adopted to examine the microscopic morphology of as-prepared samples. The TiO₂ nanoparticles (Figure 4a) show some porosity with a dense agglomeration of nanoparticles, and were irregular in shape morphology, as previously reported in the literature [34]. However, as displayed in Figure 4b, the TiO₂–CuO possesses a particular porous, netlike structure, with pores being well distributed, with an average pore-size of 20–30 microns. Meanwhile, the PANI (Figure 4c) is more irregular, possessing different shapes and sizes of agglomerates. Furthermore, it can be clearly observed that the PANI with a sphere structure and the mean void size of 20–30 nanometers are loaded on the TiO₂–CuO surfaces without agglomerates in Figure 4c.

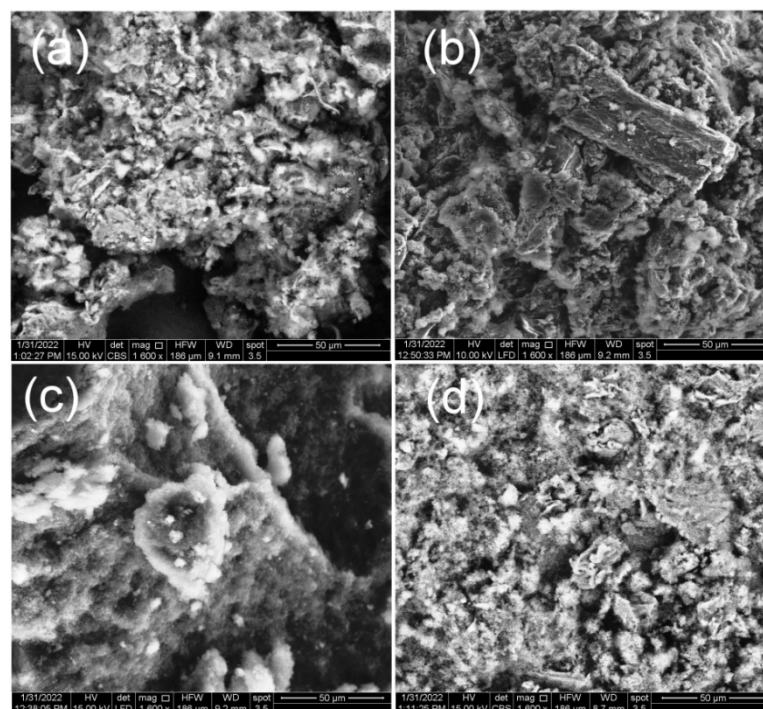


Figure 4. SEM images of: (a) TiO₂, (b) TiO₂–CuO, (c) PANI, and (d) PANI@TiO₂–CuO.

The samples are investigated using TEM and the images can be seen in Figure 5. The morphology of TiO₂ particles is a spherical shape with regular shape and a size in the scale

of 45–50 nm. As displayed in Figure 5b, the CuO spheres are uniformly distributed on the TiO₂, and the inside is brighter than the outer layer's black spheres, confirming that the formed TiO₂–CuO composite has a unique hollow structure. Nevertheless, Figure 5c shows the image of the PANI, which is formed by nanofibers with a diameter of 15–20 nm. Van der Waal's interaction caused the PANI structure to assemble into bundles. Further, the TEM image of hybrid material (Figure 5d) displays the uniform distribution of TiO₂–CuO in the PANI matrix, due to strong interfacial adhesion between both. The average diameter of PANI@TiO₂–CuO was found to be approximately 55–60 nm.

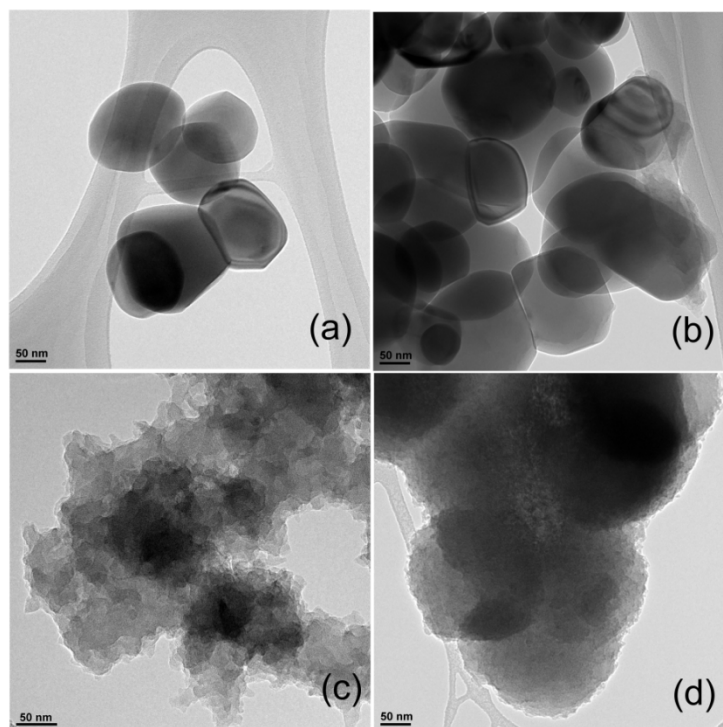


Figure 5. TEM images of: (a) TiO₂, (b) TiO₂–CuO, (c) PANI, and (d) PANI@TiO₂–CuO.

Figure 6a illustrates that the UV-Vis spectra of PANI and PANI@TiO₂–CuO. PANI has two characteristic absorption peaks; a strong band at 333 nm corresponds to π – π^* transition of the phenyl group and is attributed to the extent of conjugation along the PANI backbone. The band around 623 nm is due to the n – π^* transition of the HOMO with LUMO orbitals of the (B) ring and (Q) rings, respectively [35,36]. For hybrid material, the shape of the spectra is similar to pure PANI, but there are modifications in the intensity and absorption edge due to the efficient interaction between nanosized TiO₂–CuO and the PANI matrix. Moreover, the successful reinforcement of PANI with TiO₂–CuO is ensured by the move in absorption edges, which can be attributed to π – π^* and n – π^* electronic transitions to lower (hypo-chromic) and higher (batho-chromic) wavelengths, respectively.

The minimum energy level needed for electrons to excite from a low-energy conduction band to a high-energy valence band is the optical band gap energy (E_g). The E_g values related with PANI and PANI@TiO₂–CuO are calculated using Tauc's equation [37]:

$$(ah\nu)^n = B(h\nu - E_g) \quad (1)$$

where h is Planck's constant, B is the absorption constant, α is the absorption coefficient, and ν is the frequency of light; n is a coefficient associated with the electronic transition and can take values of ($\frac{1}{2}$ and 2) if the transition is direct or indirect, respectively. The straight line's intercept with the photon energy axis gives the E_g value of the sample and the obtained values are summarized in Figure 6b. The E_g value for PANI is 2.60 eV and

that of PANI@TiO₂-CuO is 2.27 eV, which can be ascribed to a newly formed intermediate energy level, through which facile excitation of electrons occurs [24,25].

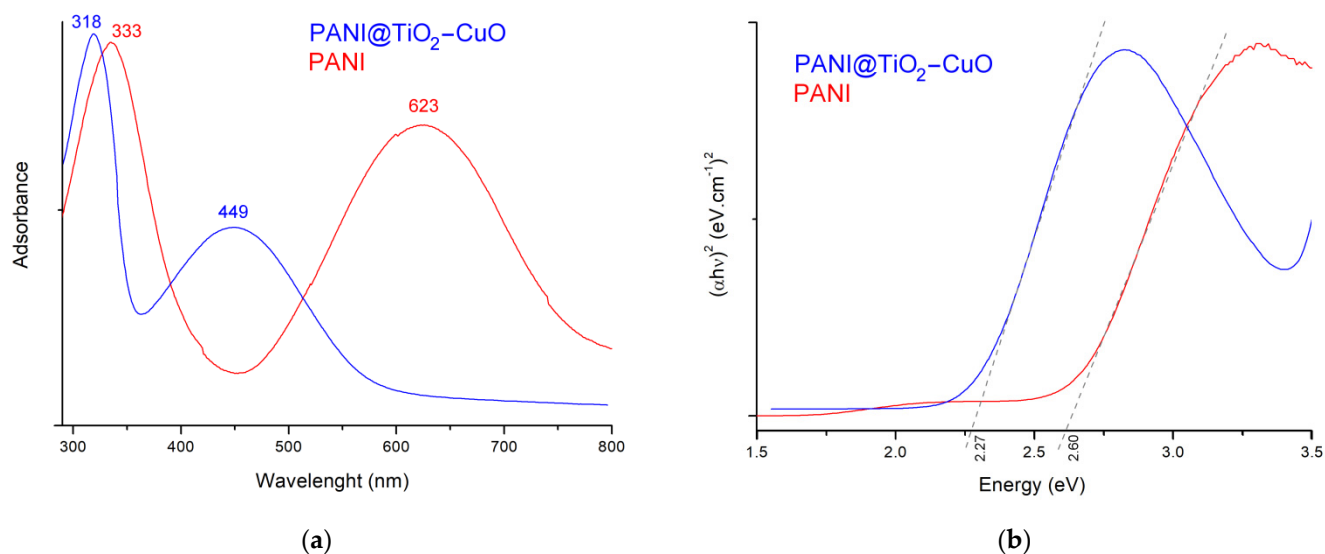


Figure 6. (a): UV-vis spectroscopy absorption spectra and (b): Tauc plots of samples.

The TGA results revealed that hybrid material shows different thermal behaviors than TiO₂-CuO or pure PANI. The thermal decomposition of samples occurred in various steps, as shown in Figure 7. The first step has a mass loss of 3.32% for PANI@TiO₂-CuO and 6.57% for PANI, which corresponds to the release of water molecules. The following steps of thermal decomposition were observed between 160 °C and 580 °C, and are associated with thermal decomposition of organic material. This result confirms the incorporation of the PANI matrix onto the TiO₂-CuO surface. Furthermore, materials decompose gradually, and a sharp weight drop takes place between 600–900 °C. This illustrates that PANI@TiO₂-CuO is more stable than PANI, but less stable than TiO₂-CuO, indicating its potential application at higher temperatures.

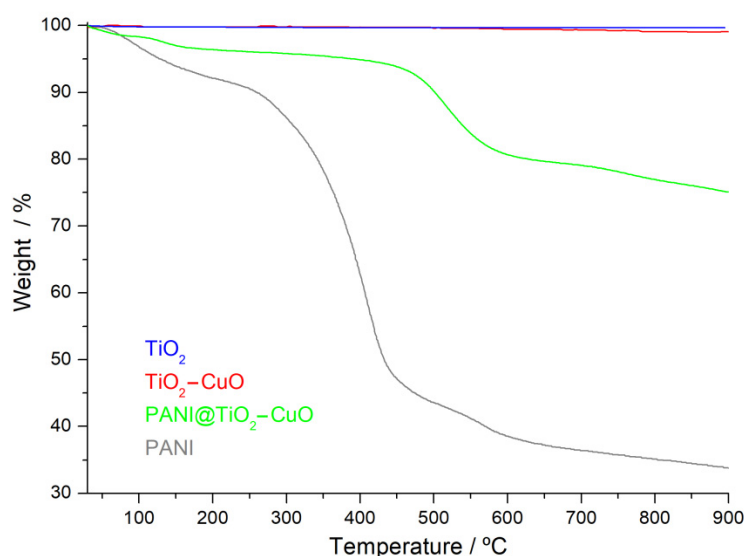


Figure 7. TGA curves of samples.

3.2. Electrochemical Properties

The comparative CV of product electrodes in 1 M HCl electrolyte at a scan rate of 50 mV s^{-1} , in the potential window of 0.0 to 1.0 V, are shown in Figure 8. The mass charge of the active samples on the material electrode is around 1 mg cm^{-2} . For the PANI sample, the first redox peak at (0.46/0.28 V) relates to the Leucoemeraldine (LE) transition to the partly oxidized Emeraldine (E), resulting in a potential peak separation (ΔE_p) close to 180 mV; and the second redox peak (0.89/0.81 V) can be attributed to the (E) transition to the entirely oxidized Pernigraniline (PA) form that presents a ΔE_p value of 80 mV [27]. Moreover, the CV of the PANI@TiO₂-CuO electrode also shows two pairs of clear redox couples that conform to the pseudocapacitive behavior of PANI. These redox pairs reveal the redox transition between (LE) and (E), and between (E) and (PA). The oxidation peak at approximately 0.38 V is due to the transformation of the (LE) to conductive (E) state. The oxidation peak at 0.67 V can be assigned to the transformation of the (E) oxidation state to a fully oxidized (PA) form. The reduction peaks at 0.50 V and 0.31 V are due to the transformation of the (E) and (LE), respectively. As anticipated, the PANI@TiO₂-CuO shows an enhanced noticeable electrical response when compared to PANI@TiO₂ and pure PANI samples, which corresponds to the synergistic impact of TiO₂-CuO and PANI as conductive fillers [38]. Meanwhile, the redox current density of this sample becomes larger and larger as the scan rate increases, indicating a good rate capability of the electrode. In other words, the formation of the PANI matrix on TiO₂-CuO causes a shift in the redox peak values toward more negative potentials compared with PANI, and this phenomenon is due to the synergetic effect of the combined contributions from both inorganic and polymer [39]. Thereby, this pairs' redox gives ΔE_p values of 70 mV and 170 mV, respectively.

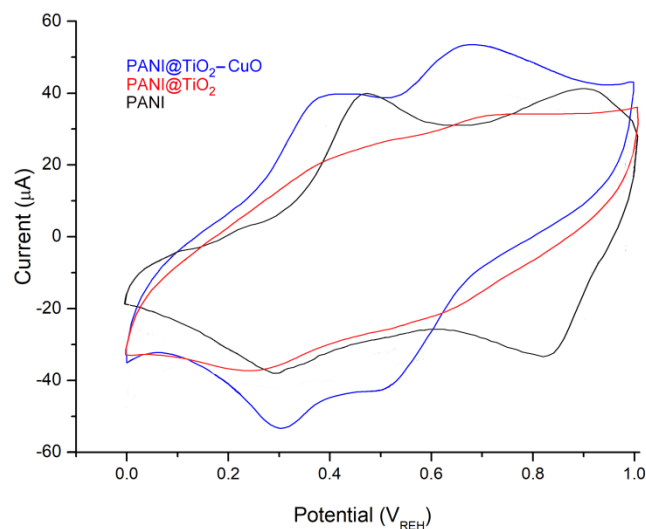


Figure 8. Cyclic voltammograms recorded for a stainless in HCl solution (1M) scan rate 50 mV s^{-1} .

Additionally, Figure 9 shows CV performance of the PANI@TiO₂-CuO, which is recorded in an electrochemical window from 0.0 V to 1.0 V at various scan rates of 5 mV s^{-1} , 10 mV s^{-1} , 20 mV s^{-1} , 30 mV s^{-1} , and 50 mV s^{-1} . The CV analysis is beneficial to further understanding the electrochemical behavior and stability during electrochemical measurement processes [40]. The area of close curves gets larger with the increase of scan rate, while the shape of CV curves exhibit Faradic redox pairs, suggesting typical pseudo capacitance and double-layer capacitive behaviors of this supercapacitor electrode.

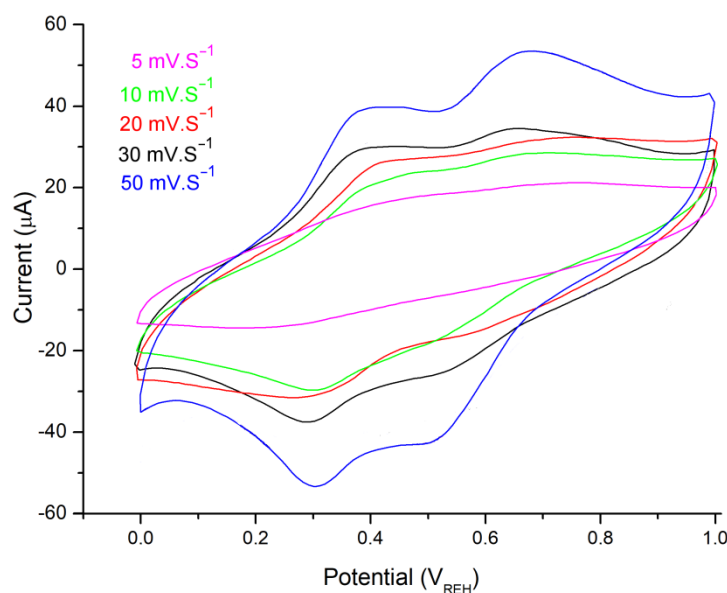


Figure 9. CV profiles of the PANI@TiO₂-CuO electrode at various sweep rates at 1.0 A g⁻¹ in HCl solution (1 M).

3.3. Galvanostatic Charge Discharge (GCD)

The charge storage properties were studied in more depth by GCD measurements. The GCD curves of the PANI@TiO₂-CuO electrode display nonlinear shape with two voltage phases in the discharge operation, and also clearly indicate electrochemical behavior at various current densities (Figure 10), showing a perfect reversibility and effective charge/ion transport of the supercapacitor [40]. At relatively smaller current densities of 1.0 mA cm⁻², the previous stage (1.0–0.5 V), with a comparatively short discharging time, corresponds to the electrochemical double layer capacitors (EDLC), while the last stage (0.5–0.0 V), with a longer discharge time, can be ascribed to an integration of EDLC and pseudo capacitor capacitance. The supercapacitor prepared using PANI@TiO₂-CuO shows areal specific capacitances of 296.7 ± 0.2, 264.1 ± 0.2, 154.6 ± 0.2, 94.7 ± 0.2, and 82.8 ± 0.2 mF cm⁻² at 1.0, 2.0, 5.0, 8.0, and 10 mA cm⁻², respectively. It is possible that a current density above 5 mA cm⁻² leads to irreversible processes [40]. Moreover, below 2 mA cm⁻² leads to an improvement in the electrode performance. A typical comparison of GCD profiles of the PANI@TiO₂ and PANI electrodes is displayed in the inset of Figure 11. Consequently, PANI@TiO₂-CuO at a current density of 1.0 mA cm⁻² displays the largest areal specific capacitance (296.7 ± 0.1 mF cm⁻²), which is better than those of PANI@TiO₂ (182.5 ± 0.1 mF cm⁻²), and PANI (195.9 ± 0.1 mF cm⁻²). Moreover, the perfect conjugated structure of PANI backbone was destroyed and the conductivity of PANI@TiO₂ decreased, due to presence of TiO₂ on polymer matrix. A low conductivity causes slow electron transmission for the redox reaction of product, and leads to a low electroactivity of PANI@TiO₂, which eventually resulted in a low specific capacitance.

To evaluate and test the workable application of electrode materials, the long-term cycling stability at a current density of 1.0 mA cm⁻² after 1500 cycles under continual GCD process is shown in Figure 11. The results suggest that the cycling stability of PANI@TiO₂-CuO electrodes have a capacitance retention of 87.5 ± 0.1%, and it is better than that of other electrodes. This is fundamentally due to the PANI matrix being focused on the axial directions of the TiO₂-CuO and being developed uniformly, with strong interfacial adhesion [41]. Conversely, PANI and PANI@TiO₂ showed lower capacitance retention of 79.3 ± 0.1% and 84.7 ± 0.1%, respectively.

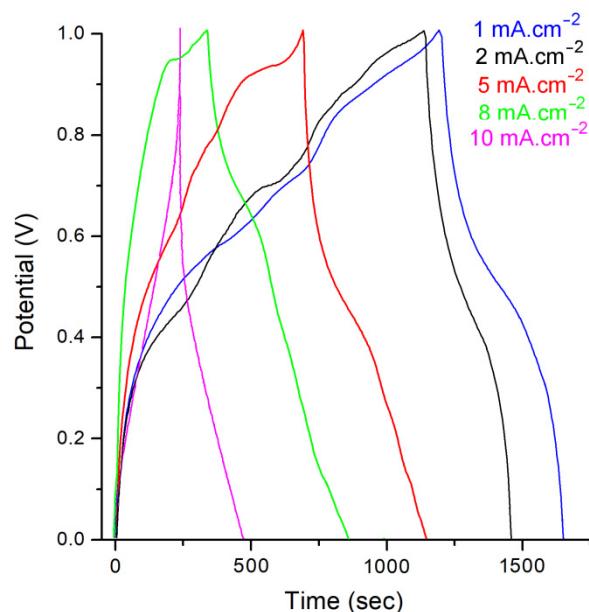


Figure 10. Galvanostatic charge–discharge (GCD) curves of the PANI@TiO₂–CuO electrode at different current densities.

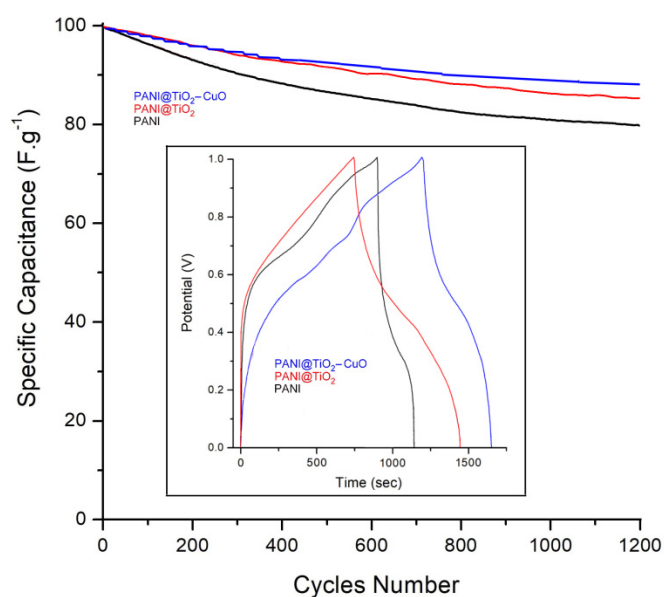


Figure 11. The cycling performance of PANI, PANI@TiO₂ and PANI@TiO₂–CuO electrodes at a current density of 1 A g^{−1}; The inset demonstrates the comparative GCD curves of PANI, PANI@TiO₂ and PANI@TiO₂–CuO at a current density of 1.0 mA cm².

4. Conclusions

The new PANI@TiO₂–CuO ternary composite was prepared via in-situ oxidative polymerization, while the TiO₂–CuO was synthesized by a process involving the preparation of CuO in the presence of TiO₂ by a facile method. The XRD technique results confirm the successful formation of TiO₂–CuO and its presence in the emeraldine phase of the PANI matrix, and the crystallinity increases with the presence of TiO₂–CuO in the ternary composite structure. The structure, morphology, and thermal properties of materials were systematically characterized using FTIR, XPS, XRD, SEM, TEM, UV-Vis, and TGA. The results indicated that TiO₂–CuO was dispersed uniformly in the PANI matrix. Due to such dispersion of the TiO₂–CuO composite, the PANI@TiO₂–CuO ternary composite

exhibits dramatic improvements compared to the neat PANI. The surface area and pore structure properties of the materials under investigation are measured by BET. Moreover, the PANI@TiO₂-CuO material shows a highly enhanced capacitance in comparison with PANI and PANI@TiO₂. This superior capacitance results from the combination of electrochemical behaviors of PANI and TiO₂-CuO. The ternary composite shows long-term cycling stability without any noticeable degradation for over 1500 cycles. These findings provide a facile strategy to prepare hybrid materials of PANI and TiO₂-CuO with a highly improved capacitance, which we believe will have possible applications in the future.

Author Contributions: Conceptualization: N.B., H.D., I.M. and F.Z.D.; methodology: N.B., H.D. and F.Z.D.; software: N.B. and A.B.; validation: L.S. and A.B.; visualization: H.D. and L.S.; formal analysis: N.B. and A.B.; investigation: N.B., H.D., F.Z.D., L.S. and A.B.; data curation: N.B.; writing—original draft preparation: N.B., H.D., I.M. and L.S.; writing—review and editing, all authors; supervision, A.B. All authors have read and agreed to the published version of the manuscript.

Funding: This research received no external funding.

Institutional Review Board Statement: Not applicable.

Data Availability Statement: Not applicable.

Acknowledgments: We would like to thank DGRSDT-MESRS of Algeria for their financial support. We also thank Ana-Katrina Büttner for language editing. The author (A. Benyoucef) would like to acknowledge IUMA of Alicante University Spain researchers for their support and co-operation.

Conflicts of Interest: The authors declare no conflict of interest.

References

1. Verma, S.; Das, T.; Pandey, V.K.; Verma, B. Nanoarchitectonics of GO/PANI/CoFe₂O₄ (Graphene Oxide/polyaniline/Cobalt Ferrite) based hybrid composite and its use in fabricating symmetric supercapacitor devices. *J. Mol. Struct.* **2022**, *1266*, 133515. [[CrossRef](#)]
2. Navarro, N.C.R.; Kajiura, R.; Miura, A.; Tadanaga, K. Organic-Inorganic Hybrid Materials for Interface Design in All-Solid-State Batteries with a Garnet-Type Solid Electrolyte. *ACS Appl. Energy Mater.* **2020**, *3*, 11260–11268. [[CrossRef](#)]
3. Yang, L.; Pan, L.; Xiang, H.; Fei, X.; Zhu, M. Organic-Inorganic Hybrid Conductive Network to Enhance the Electrical Conductivity of Graphene-Hybridized Polymeric Fibers. *Chem. Mater.* **2022**, *34*, 2049–2058. [[CrossRef](#)]
4. Maity, N.; Ghosh, R.; Nandi, A.K. Optoelectronic Properties of Self-Assembled Nanostructures of Polymer Functionalized Polythiophene and Graphene. *Langmuir* **2018**, *34*, 7585–7597. [[CrossRef](#)]
5. Miyashita, R.; Goto, H. Electro-Magneto-Optically Active Polyaniline/Hydroxypropyl Cellulose Composite. *ACS Appl. Polym. Mater.* **2022**, *4*, 796–805. [[CrossRef](#)]
6. Yang, M.; Liu, Y.; Luo, X.; Cao, Y.; Gong, X.; Xu, W. Molecular Engineering of Polyaniline with Ultrathin Polydopamine and Monolayer Graphene for All-Solid-State Flexible Microsupercapacitors. *ACS Appl. Energy Mater.* **2021**, *4*, 10069–10080. [[CrossRef](#)]
7. Beygisangchin, M.; Abdul Rashid, S.; Shafie, S.; Sadrolhosseini, A.R.; Lim, H.N. Preparations, Properties, and Applications of Polyaniline and Polyaniline Thin Films—A Review. *Polymers* **2021**, *13*, 2003. [[CrossRef](#)] [[PubMed](#)]
8. Firda, P.B.D.; Malik, Y.T.; Oh, J.K.; Wujcik, E.K.; Jeon, J.W. Enhanced Chemical and Electrochemical Stability of Polyaniline-Based Layer-by-Layer Films. *Polymers* **2021**, *13*, 2992. [[CrossRef](#)]
9. Rajkumar, S.; Ezhilarasi, J.C.; Saranya, P.; Merlin, J.P. Fabrication of CoWO₄/PANI composite as electrode material for energy storage applications. *J. Phys. Chem. Solids* **2022**, *162*, 110500. [[CrossRef](#)]
10. Lahreche, S.; Moulefera, I.; El Kebir, A.; Sabantina, L.; Kaid, M.; Benyoucef, A. Application of Activated Carbon Adsorbents Prepared from Prickly Pear Fruit Seeds and a Conductive Polymer Matrix to Remove Congo Red from Aqueous Solutions. *Fibers* **2022**, *10*, 7. [[CrossRef](#)]
11. Daikh, S.; Ouis, D.; Benyoucef, A.; Mouffok, B. Equilibrium, kinetic and thermodynamic studies for evaluation of adsorption capacity of a new potential hybrid adsorbent based on polyaniline and chitosan for Acetaminophen. *Chem. Phys. Lett.* **2022**, *17*, 139565. [[CrossRef](#)]
12. Song, Y.; Su, Z.; Zhao, Z.; Lin, S.; Wang, D. A new As₃Mo₈V₄/PANI/rGO composite for high performance supercapacitor electrode. *Ceram. Int.* **2021**, *47*, 21367–21372. [[CrossRef](#)]
13. Maaza, L.; Djafri, F.; Belmokhtar, A.; Benyoucef, A. Evaluation of the influence of Al₂O₃ nanoparticles on the thermal stability and optical and electrochemical properties of PANI-derived matrix reinforced conducting polymer composites. *J. Phys. Chem. Solids* **2021**, *152*, 109970. [[CrossRef](#)]
14. Feng, Q.; Zhang, H.; Shi, Y.; Yu, X.; Lan, G. Preparation and Gas Sensing Properties of PANI/SnO₂ Hybrid Material. *Polymers* **2021**, *13*, 1360. [[CrossRef](#)]

15. Xiao, T.; Zhao, J.; Wang, X.; Li, Z.; Song, M.; Li, H.; Wang, X. Preparation and performance of PANI-TiO₂ nanotube arrays composite electrode by in-situ microcavity polymerization. *Mater. Chem. Phys.* **2020**, *240*, 122179. [[CrossRef](#)]
16. Shao, Z.; Li, H.; Li, M.; Li, C.; Qu, C.; Yang, B. Fabrication of polyaniline nanowire/TiO₂ nanotube array electrode for supercapacitors. *Energy* **2015**, *87*, 578–585. [[CrossRef](#)]
17. Belhadj, H.; Moulefera, I.; Sabantina, L.; Benyoucef, A. Effects of Incorporating Titanium Dioxide with Titanium Carbide on Hybrid Materials Reinforced with Polyaniline: Synthesis, Characterization, Electrochemical and Supercapacitive Properties. *Fibers* **2022**, *10*, 46. [[CrossRef](#)]
18. Prakash, J.; Kumar, A.; Dai, H.; Janegitz, B.C.; Krishnan, V.; Swart, H.C.; Sun, S. Novel rare earth metal-doped one-dimensional TiO₂ nanostructures: Fundamentals and multifunctional applications. *Mater. Today Sustain.* **2021**, *13*, 100066. [[CrossRef](#)]
19. Deshmukh, P.R.; Patil, S.V.; Bulakhe, R.N.; Pusawale, S.N.; Shim, J.J.; Lokhande, C.D. Chemical synthesis of PANI-TiO₂ composite thin film for supercapacitor application. *RSC Adv.* **2015**, *5*, 68939–68946. [[CrossRef](#)]
20. Gottam, R.; Srinivasan, P.; Keloth, B. Improving the Performance of PANI-SA·TiO₂ Supercapacitor Active Electrode Material via Emulsion Polymerization of Aniline with MWCNT. *ChemistrySelect* **2020**, *5*, 10098–10105. [[CrossRef](#)]
21. Yoruk, O.; Bayrak, Y.; Ates, M. Design and assembly of supercapacitor based on reduced graphene oxide/TiO₂/polyaniline ternary nanocomposite and its application in electrical circuit. *Polym. Bull.* **2022**, *79*, 2969–2993. [[CrossRef](#)]
22. Kumar, N.; Joshi, N.C. Adsorption applications of synthetically prepared PANI-CuO based nanocomposite material. *J. Indian Chem. Soc.* **2022**, *99*, 100551. [[CrossRef](#)]
23. Liu, T.; Guo, Y.; Zhang, Z.; Miao, Z.; Zhang, X.; Su, Z. Fabrication of hollow CuO/PANI hybrid nanofibers for non-enzymatic electrochemical detection of H₂O₂ and glucose. *Sens. Actuators B Chem.* **2019**, *286*, 370–376. [[CrossRef](#)]
24. Nekooie, R.; Shamspur, T.; Mostafavi, A. Novel CuO/TiO₂/PANI nanocomposite: Preparation and photocatalytic investigation for chlorpyrifos degradation in water under visible light irradiation. *J. Photochem. Photobiol. A Chem.* **2021**, *407*, 113038. [[CrossRef](#)]
25. Pang, Z.; Nie, Q.; Lv, P.; Yu, J.; Huang, F.; Wei, Q. Design of flexible PANI-coated CuO-TiO₂-SiO₂ heterostructure nanofibers with high ammonia sensing response values. *Nanotechnology* **2017**, *28*, 225501. [[CrossRef](#)]
26. Nguyen, T.H.; Nguyen, T.L.; Ung, T.D.T.; Nguyen, Q.L. Synthesis and characterization of nano-CuO and CuO/TiO₂ photocatalysts. *Adv. Nat. Sci. Nanosci. Nanotechnol.* **2013**, *4*, 025002. [[CrossRef](#)]
27. Bekhoukh, A.; Moulefera, I.; Sabantina, L.; Benyoucef, A. Development, Investigation, and Comparative Study of the Effects of Various Metal Oxides on Optical Electrochemical Properties Using a Doped PANI Matrix. *Polymers* **2021**, *13*, 3344. [[CrossRef](#)]
28. Dong, Y.; Zhao, Z.; Wang, Z.; Liu, Y.; Wang, X.; Qiu, J. Dually Fixed SnO₂ Nanoparticles on Graphene Nanosheets by Polyaniline Coating for Superior Lithium Storage. *ACS Appl. Mater. Interfaces* **2015**, *7*, 2444–2451. [[CrossRef](#)]
29. Rathore, B.S.; Chauhan, N.P.S.; Jadoun, S.; Ameta, S.C.; Ameta, R. Synthesis and characterization of chitosan-polyaniline-nickel(II) oxide nanocomposite. *J. Mol. Struct.* **2021**, *1242*, 130750. [[CrossRef](#)]
30. Sumana, V.S.; Sudhakar, Y.N.; Varghese, A.; Nagaraja, G.K. Pt nanoflower-poly(aniline) electrode material with the synchronized concept of energy storage in supercapacitor. *Appl. Surf. Sci.* **2022**, *589*, 152994. [[CrossRef](#)]
31. Radoičić, M.B.; Milošević, M.V.; Miličević, D.S.; Suljovrujić, E.H.; Marjanović, G.N.Ć.; Radetić, M.M.; Šaponjić, Z.V. Influence of TiO₂ nanoparticles on formation mechanism of PANI/TiO₂ nanocomposite coating on PET fabric and its structural and electrical properties. *Surf. Coat. Technol.* **2015**, *278*, 38–47. [[CrossRef](#)]
32. Girimonte, R.; Testa, F.; Turano, M.; Leone, G.; Gallo, M.; Golemme, G. Amine-Functionalized Mesoporous Silica Adsorbent for CO₂ Capture in Confined-Fluidized Bed: Study of the Breakthrough Adsorption Curves as a Function of Several Operating Variables. *Processes* **2022**, *10*, 422. [[CrossRef](#)]
33. Toumi, I.; Djelad, H.; Chouli, F.; Benyoucef, A. Synthesis of PANI@ZnO Hybrid Material and Evaluations in Adsorption of Congo Red and Methylene Blue Dyes: Structural Characterization and Adsorption Performance. *J. Inorg. Organomet. Polym. Mater.* **2022**, *32*, 112–121. [[CrossRef](#)]
34. Anandgaonker, P.; Kulkarni, G.; Gaikwad, S.; Rajbhoj, A. Synthesis of TiO₂ nanoparticles by electrochemical method and their antibacterial application. *Arab. J. Chem.* **2019**, *12*, 1815–1822. [[CrossRef](#)]
35. Wang, H.; Xie, Y. Hydrogen bond enforced polyaniline grown on activated carbon fibers substrate for wearable bracelet supercapacitor. *J. Energy Storage* **2022**, *52*, 105042. [[CrossRef](#)]
36. Gharahcheshmeh, M.H.; Gleason, K.K. Recent Progress in Conjugated Conducting and Semiconducting Polymers for Energy Devices. *Energies* **2022**, *15*, 3661. [[CrossRef](#)]
37. Radja, I.; Djelad, H.; Morallon, E.; Benyoucef, A. Characterization and electrochemical properties of conducting nanocomposites synthesized from p-anisidine and aniline with titanium carbide by chemical oxidative method. *Synth. Met.* **2015**, *202*, 25–32. [[CrossRef](#)]
38. Ge, D.; Yang, L.; Fan, L.; Zhang, C.; Xiao, X.; Gogotsi, Y.; Yang, S. Foldable supercapacitors from triple networks of macroporous cellulose fibers, single-walled carbon nanotubes and polyaniline nanoribbons. *Nano Energy* **2015**, *11*, 568–578. [[CrossRef](#)]
39. Gautam, K.P.; Acharya, D.; Bhatta, I.; Subedi, V.; Das, M.; Neupane, S.; Kunwar, J.; Chhetri, K.; Yadav, A.P. Nickel Oxide-Incorporated Polyaniline Nanocomposites as an Efficient Electrode Material for Supercapacitor Application. *Inorganics* **2022**, *10*, 86. [[CrossRef](#)]

-
40. Gallagher, K.G.; Trask, S.E.; Bauer, C.; Woehrle, T.; Lux, S.F.; Tschuch, M.; Lamp, P.; Polzin, B.J.; Ha, S.; Long, B.; et al. Optimizing areal capacities through understanding the limitations of lithium-ion electrodes. *J. Electrochem. Soc.* **2016**, *163*, A138–A149. [[CrossRef](#)]
 41. Yang, X.; Qiu, Y.; Zhang, M.; Zhang, L.; Li, H. Facile Fabrication of Polyaniline/Graphene Composite Fibers as Electrodes for Fiber-Shaped Supercapacitors. *Appl. Sci.* **2021**, *11*, 8690. [[CrossRef](#)]